Author/s:
Akasaka, H;Nakahana, M;Nakayama, M;Morita, K;Salah, M;Mukumoto, N;Shimizu, Y;Zhangzhu, R;Ogino, C;Cortez-Jugo, C;Richardson, JJ;Caruso, F;Sasaki, R

Title:
Polyphenol-Mediated Antibody Functionalization of Titanium Peroxide Nanoparticles for Cancer Cell Targeting

Date:
2025

Citation:
Akasaka, H., Nakahana, M., Nakayama, M., Morita, K., Salah, M., Mukumoto, N., Shimizu, Y., Zhangzhu, R., Ogino, C., Cortez-Jugo, C., Richardson, J. J., Caruso, F. & Sasaki, R. (2025). Polyphenol-Mediated Antibody Functionalization of Titanium Peroxide Nanoparticles for Cancer Cell Targeting. ACS Applied Bio Materials, 8 (12), pp.A-L. https://doi.org/10.1021/acsabm.5c01645.

Persistent Link:
https://hdl.handle.net/11343/361480

ACS APPLIED BIO MATERIALS

www.acsabm.org
Article

Polyphenol-Mediated Antibody Functionalization of Titanium Peroxide Nanoparticles for Cancer Cell Targeting

Hiroaki Akasaka, Makiko Nakahana, Masao Nakayama, Kenta Morita, Mohammed Salah, Naritoshi Mukumoto, Yasuyuki Shimizu, Ruixain Zhangzhu, Chiaki Ogino, Christina Cortez-Jugo, Joseph J. Richardson, Frank Caruso, and Ryohei Sasaki*

Cite This: https://doi.org/10.1021/acsabm.5c01645

Read Online

ACCESS | Metrics & More | Article Recommendations | Supporting Information

ABSTRACT: Cell targeting would benefit various biotechnological applications such as disease diagnosis and cancer therapy. However, efficiently functionalizing nanoparticles with targeting ligands such as antibodies remains challenging. For example, poly(acrylic acid)-modified titanium peroxide NPs (PAATiO*x*) have shown promising radiosensitizing effects but suffer from poor tumor accumulation due to a lack of targeting. Herein, we developed a simple, one-pot process to noncovalently graft anti-CD44 antibodies onto the surface of PAATiO*x* NPs using tannic acid, a polyphenol that can bind to diverse surfaces and biomolecules via multiple molecular interactions. We evaluated the cellular binding, internalization, therapeutic efficacy, and biodistribution of the targeted particles. The antibody-functionalized NPs exhibited ∼2-fold enhanced binding to CD44-expressing cells compared to unmodified NPs and enhanced cellular internalization in vitro (2.4-fold in MIAPaCa-2 cells and 6.5-fold in MDA-MB-231 cells). Additionally, the NPs maintained their radiosensitizing property, significantly inhibiting the growth of CD44-expressing cells by 2-fold compared with CD44-negative cells. In vivo biodistribution studies revealed ∼2-fold greater tumor accumulation of the targeted NPs compared to unmodified NPs ($p < 0.05$). This polyphenol-mediated antibody coating strategy is a versatile and broadly applicable platform for enhancing nanoparticle delivery to specific cell populations, with potential for improving radiotherapy outcomes in CD44-positive tumors.

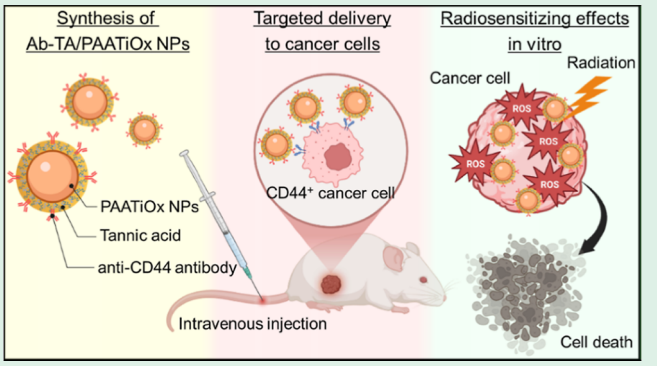

KEYWORDS: *radiotherapy, nanoparticles, radiation sensitizer, drug delivery systems, phenolics, metal−phenolic networks*

INTRODUCTION

Cancer is a leading cause of mortality worldwide, necessitating diverse treatment approaches, including surgery, chemotherapy, immunotherapy, and radiotherapy. Among these approaches, radiotherapy has demonstrated promise for specific malignancies such as head and neck cancers.[1−4] However, the therapeutic efficacy of radiotherapy faces two significant limitations: (1) radiation dose constraints due to potential damage to surrounding healthy tissue[5] and (2) the persistence of cancer stem cells following treatment, which can lead to relapse, metastasis, and multidrug resistance.[6] To address these challenges, research has increasingly focused on developing radiosensitizing agents that can enhance the efficacy of radiotherapy while minimizing off-target damage to healthy tissues.[7−9] For example, we have recently shown that nanoparticles made from poly(acrylic acid)-modified titanium peroxide (PAATiO*x*) have radiosensitizing effects,[10−12] and local administration of these NPs into the tumor of a mouse xenograft model significantly enhances X-ray therapeutic effects.[10,12] However, biodistribution studies revealed that only 10% of the injected NPs accumulated within the tumors.[13] This limited tumor accumulation represents a critical barrier to maximizing therapeutic efficacy, underscoring the need for targeted delivery strategies that can direct PAATiO*x* NPs specifically to cancer cells.

Cell targeting represents a fundamental requirement across numerous biomedical applications beyond cancer therapy, including disease diagnosis, cell sorting, microbe detection, and various biotechnological assays. Recent advances in nanotheranostics have highlighted the potential of metal−phenolic networks (MPNs) as versatile platforms for biomedical applications. MPNs exhibit tunable redox, coordination, and interfacial properties that can be precisely engineered through the selection of plant-derived polyphenols such as tannic

Received: August 22, 2025
Revised: October 28, 2025
Accepted: October 28, 2025

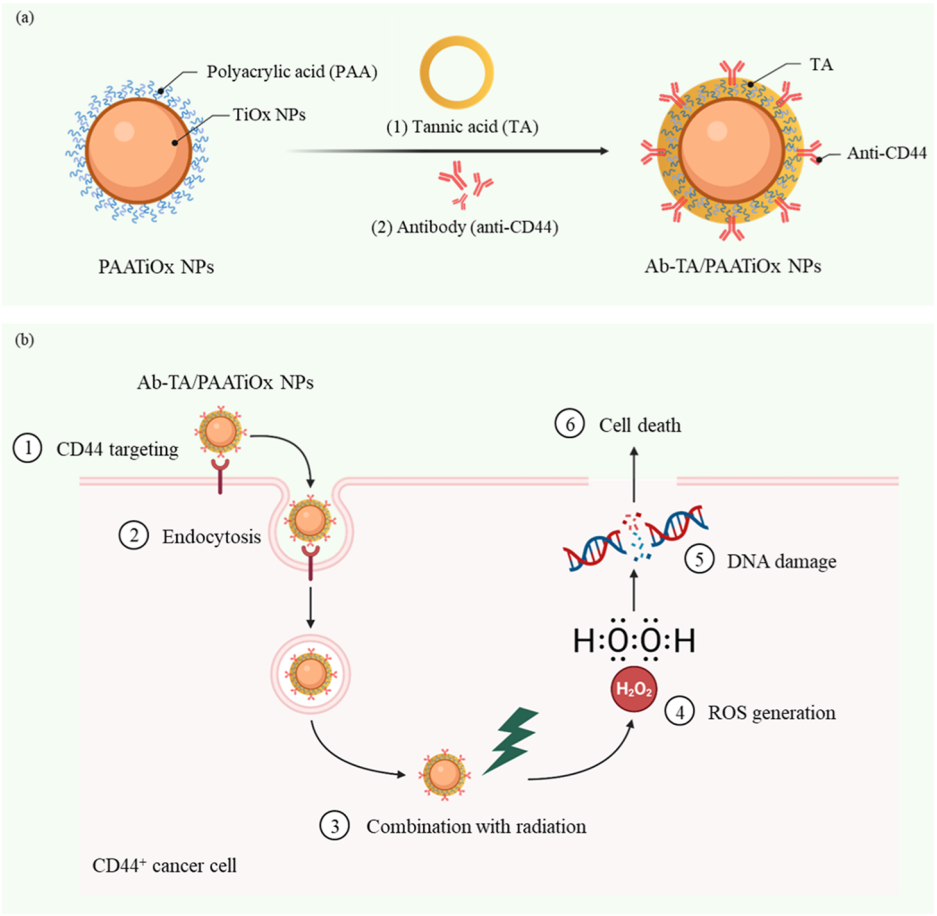

Figure 1. (a) Schematic diagram of antibody–tannic acid (Ab-TA) network coating of poly(acrylic acid)-modified titanium peroxide (PAATiO*x*) NPs to form Ab-TA/PAATiO*x* NPs. (b) Mechanism of cell death induced by Ab-TA/PAATiO*x* NPs when exposed to X-ray radiation.

acid.[14,15] In this context, the antibody–tannic acid (Ab–TA)/PAATiO*x* NPs developed in this study can be regarded as a hybrid system that integrates the metal–phenolic interface with biological targeting functionality, thus offering a structurally stable and bioresponsive radiosensitizer platform. Although specific cellular targeting can be achieved using diverse molecular entities, such as small molecules, polymers, nucleic acids, peptides, and proteins, antibodies remain the clinically preferred class of targeting molecules owing to their specificity and biocompatibility. Nevertheless, the conjugation of antibodies to nano, micro, and macro-surfaces has traditionally presented challenges, often requiring complex, costly procedures involving potentially toxic chemicals or denaturing reagents. Building on our advances in the development of universally adherent metal–phenolic networks, we recently pioneered the use of polypeptide–polyphenol networks (PPNs),[16] which are also applicable to proteins, enabling the noncovalent conjugation of proteins to surfaces under mild, ambient conditions. Polyphenols exhibit multiple interactions with proteins, including hydrogen bonding, hydrophobic interactions, and ionic interactions. These interactions enable the formation of robust and responsive protein–polyphenol networks.[16]

In the present study, we exploited the radiosensitizing properties of our PAATiO*x* NPs platform and binding properties of PPNs to develop antibody-based PPN-functionalized PAATiO*x* NPs to selectively target cancer cells. We focused on CD44 as our molecule target, as it is a cell–surface glycoprotein highly expressed in cancer stem cells.[17,18] Moreover, CD44 represents a suitable target for cancer-directed therapies as it participates in multiple cellular processing and cellular pathways, including adhesion, migration, proliferation, motility, and differentiation.[19,20] Furthermore, numerous malignancies characterized by CD44 overexpression have been the subject of extensive preclinical and clinical trials employing anti-CD44 antibodies.[21,22] By combining anti-CD44 antibodies with tannic acid (TA), we synthesized CD-44 targeting PPNs, termed Ab-TA, on PAATiO*x* NPs (Figure 1). Ab-TA coating enabled the PAATiO*x* NPs to specifically recognize CD44-expressing cancer cells, thereby facilitating nanoparticle internalization. These internalized NPs could still function as localized radiosensitizing agents that selectively enhance radiotherapy toxicity in cancer cells compared with cells with low CD44 expression. This study establishes the viability of polyphenol-mediated antibody functionalization as a platform technology for enhancing the targeted delivery of radiosensitizing NPs, thereby potentially improving radiotherapy outcomes while reducing off-target effects.

RESULTS AND DISCUSSION

The PAATiO*x* NPs were coated with anti-CD44 antibody and TA using our previously published method.[16] Briefly, TA and anti-CD44 antibody were added sequentially to PAATiO*x* NPs. Following 4 h of incubation, the resulting NPs were purified by centrifugation to obtain Ab-TA/PAATiO*x* particles

https://doi.org/10.1021/acsabm.5c01645
ACS Appl. Bio Mater. XXXX, XXX, XXX–XXX

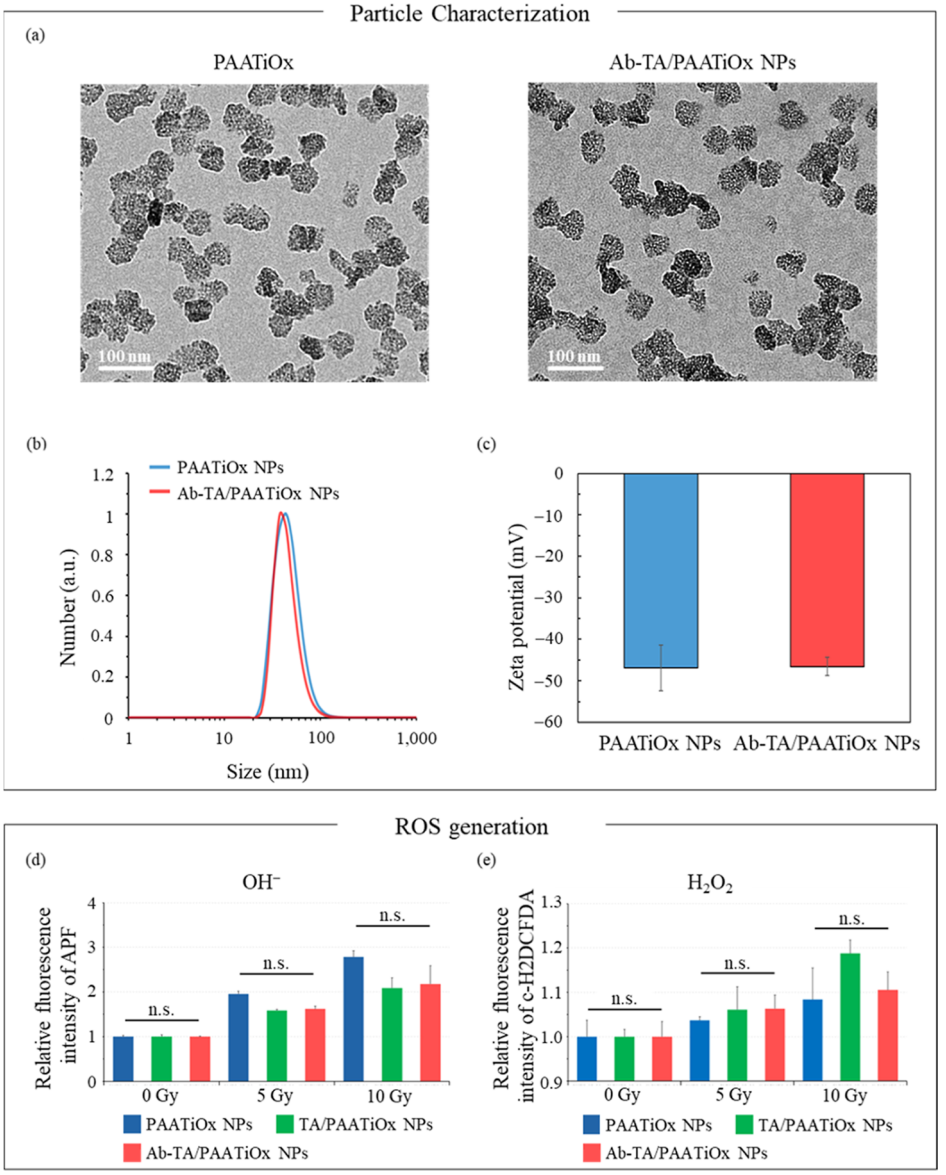

Figure 2. Characterization of unmodified and Ab-TA-coated PAATiO*x* NPs. (a) Representative transmission electron microscopy images of PAATiO*x* and Ab-TA/PAATiOx NPs. Scale bars are 100 nm. (b) Size distribution of PAATiO*x* and Ab-TA/PAATiO*x* NPs measured by DLS. (c) Zeta-potential of PAATiO*x* and Ab-TA/PAATiO*x* NPs measured in Milli-Q water (mean ± standard deviation (SD), n = 3). (d,e) ROS production by PAATiO*x*, TA/PAATiO*x*, and Ab-TA/PAATiO*x* NPs under increasing X-ray irradiation doses, as measured by hydroxyl radical (d) or hydrogen peroxide (e) formation. Aminophenylfluorescein (APF) intensity indicating hydroxyl radical production and carboxy-2′,7′-dichlorodihydrofluorescein diacetate (c-H2DCFDA) intensity indicating hydrogen peroxide production, respectively. Data are shown as the mean ± standard deviation and n = 3. Differences between groups were analyzed using the Kruskal−Wallis test with Mann−Whitney U test. Results were considered significant at $p < 0.05$.

(Figure 1). No distinct aggregation was detected before or after coating (Figure 2a), and the Ab-TA/PAATiO*x* particles were almost the same size as the unmodified PAATiO*x* NPs (Figure 2b).[23] Specifically, both PAATiO*x* and Ab-TA/PAATiO*x* NPs were ∼50 nm in diameter (air-dried), as determined by transmission electron microscopy, and 50−100 nm in diameter when hydrated, as determined by dynamic light scattering (DLS), and the polydispersity index (PDI) was 0.160 for PAATiO*x* and 0.129 for Ab-TA/PAATiO*x* NPs, respectively. The diameter of the Ab-TA/PAATiO*x* NPs aligns with optimal dimensions for cellular uptake while avoiding rapid clearance from circulation, consistent with previous reports for nanoparticle delivery systems.[24] Surface charge analysis revealed no significant difference between the zeta-potential of PAATiO*x* NPs (47 ± 6 mV) and that of Ab-TA/PAATiO*x* NPs (47 ± 2 mV) (Figure 2c). The efficiency of anti-CD44 antibody coating was 99%, with 190 antibodies coated on each nanoparticle (Table S1). ROS generation is a fundamental mechanism underlying cell death induced by the radiosensitizing effect of PAATiO*x* NPs. At X-ray irradiation doses up to 10 Gy, there was no significant difference in $^{\bullet}OH$ radical and H_2O_2 generation from PAATiO*x*, tannic acid coating PAATiO*x* (TA/PAATiO*x*), and Ab-TA/PAATiO*x* NPs in a cell-free assay. Although within the range of no significant difference, a slight decrease in $^{\bullet}OH$ radical generation was observed in Ab-TA/PAATiO*x* and TA/PAATiO*x* NPs compared with PAATiO*x* NPs, likely owing to the reductive property of TA (Figure 2d). The opposite was

https://doi.org/10.1021/acsabm.5c01645
ACS Appl. Bio Mater. XXXX, XXX, XXX−XXX

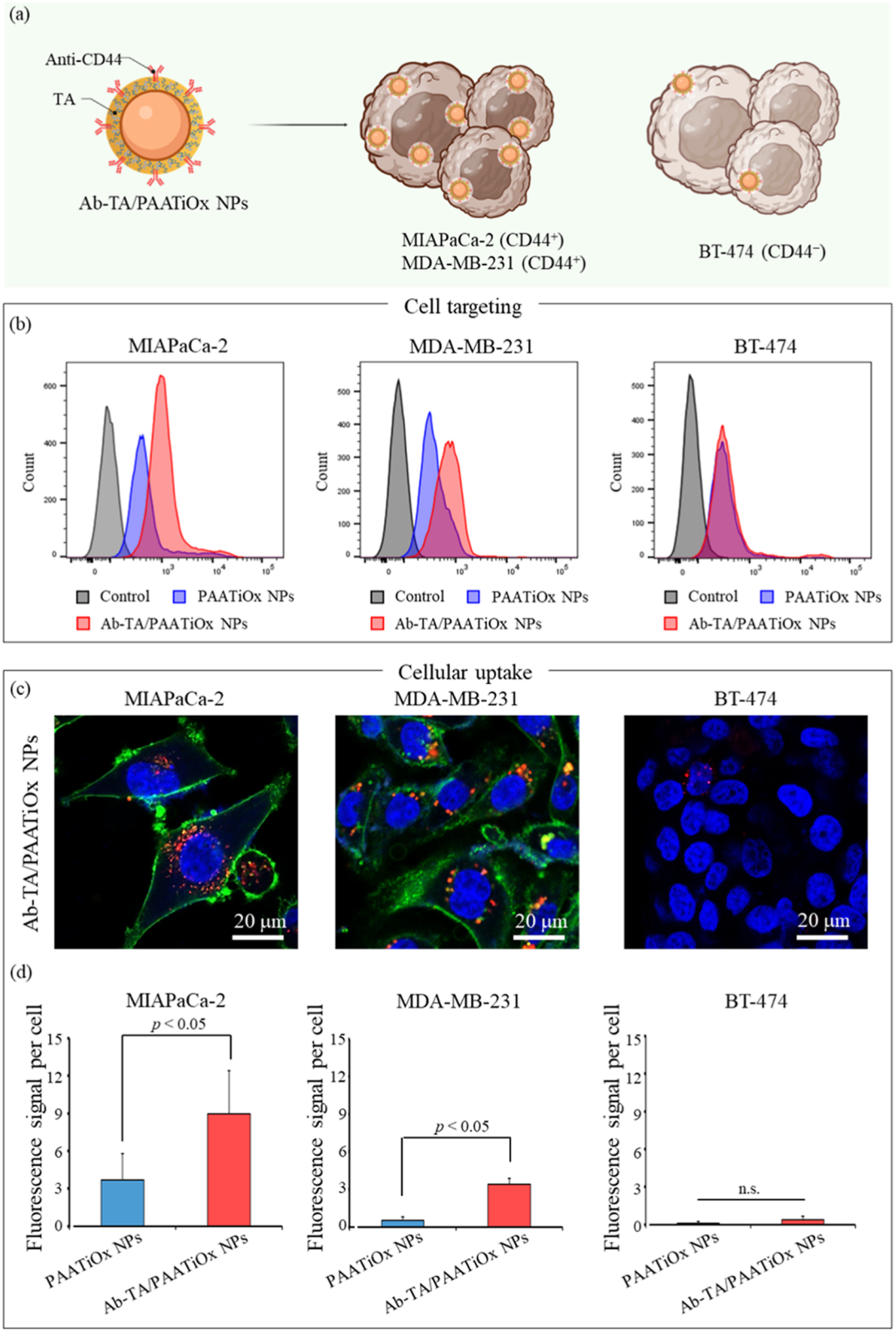

Figure 3. (a) Schematic illustration of the targeting specificity of Ab-TA/PAATiO*x* NPs toward CD44-overexpressing ($CD44^+$) cells (MIAPaCa-2 and MDA-MB-231) and CD44-low/negative ($CD44^-$) cells (BT-474). (b) Flow cytometry analysis of PAATiO*x* or Ab-TA/PAATiO*x* NPs association with cancer cell lines. (c) Fluorescence microscopy images of CD44-enriched and CD44-deficient cells. Cell nuclei are labeled blue. CD44 expressed on the surface of cancer cells is labeled green. PAATiO*x* NPs are labeled red. Scale bars are 20 μm. (d) Number of fluorescence signals per cell, obtained from microscopy images (mean ± SD, n = 3. Differences between groups were analyzed using the Kruskal−Wallis test with Mann−Whitney U test.

https://doi.org/10.1021/acsabm.5c01645
ACS Appl. Bio Mater. XXXX, XXX, XXX−XXX

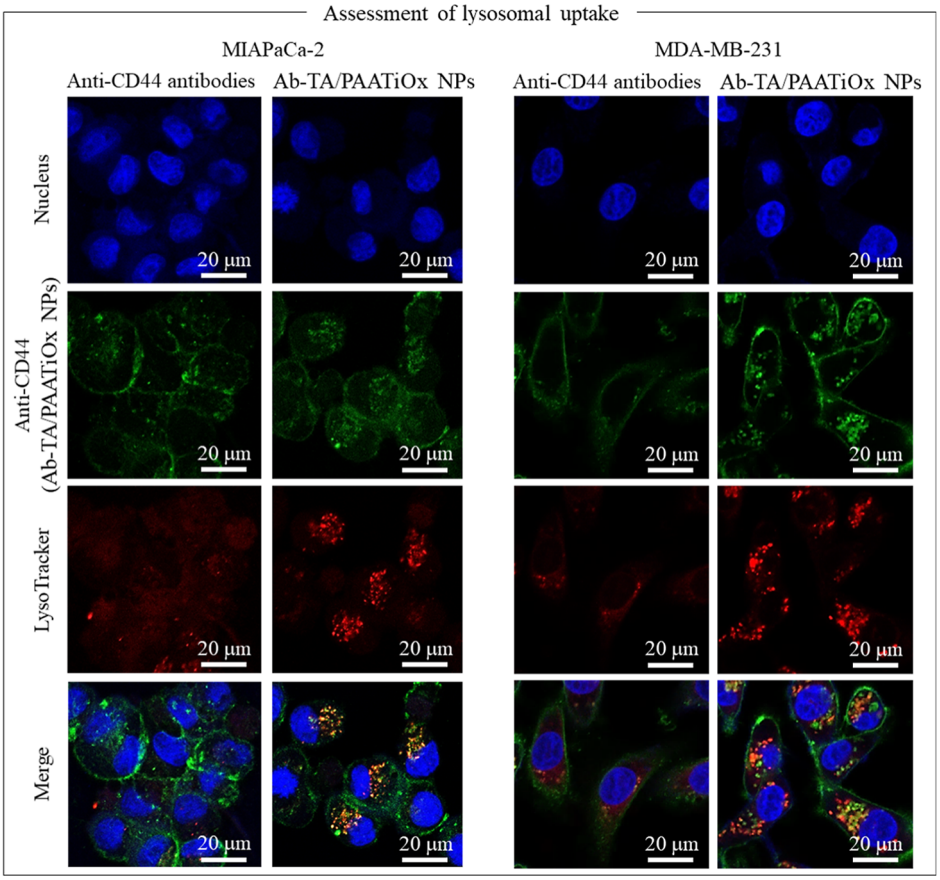

Figure 4. Endosome−lysosome colocalization of Ab-TA/PAATiO*x* NPs in $CD44^+$ cancer cell lines after 24 h incubation at 37 °C. Nuclei are labeled blue. The Ab-TA/PAATiO*x* NPs prepared with FITC-anti-CD44 are labeled green. Lysosomes labeled with LysoTracker are red. Scale bars are 20 μm.

observed with regards to H_2O_2 generation, however, which was slightly higher in TA- and Ab-TA-coated PAATiO*x* NPs (Figure 2e). Regardless, these results suggest that Ab-TA coating has negligible effect on the surface charge and, in a cell-free system, has limited effect on the functional properties of the core PAATiO*x* NPs, which maintain their radiosensitizing capability even after coating.

For cell targeting studies and biodistribution studies, the PAATiO*x* NPs were labeled with Alexa Fluor 647 (AF647), which was confirmed by flow cytometry analysis (Figure S1 and Table S2). The nonlabeled PAATiO*x* NPs exhibited no fluorescence signal (Figure S1a) unlike the AF647-labeled PAATiO*x* NPs, which showed a strong fluorescence signal (Figure S1b). Ab-TA modification was also demonstrated by incubating AF647-labeled PAATiO*x* NPs with TA and fluorescein isothiocyanate-labeled immunoglobulin G. Figure S1c confirmed successful Ab-TA surface modification of the fluorescently labeled PAATiO*x* NPs.

To evaluate whether the Ab-TA coating preserved the functionality of the antibody, we conducted targeting experiments with CD44-overexpressing cells (MIAPaCa-2, MDA-MB-231) and CD44-low/negative cells (BT-474). Anti-CD44 antibodies specifically recognize and bind to CD44-overexpressing ($CD44^+$) cells, while showing minimal interactions with cells that express low or negligible levels of CD44 ($CD44^-$) (Figure 3a). We first confirmed the surface-expression levels of CD44 by flow cytometry, where binding of anti-CD44 was detected in MIAPaCa-2 and MDA-MB-231 cell lines ($CD44^+$), but not in the low-expressing BT-474 cells ($CD44^-$) (Figure S2 and Table S3). Nanoparticle−cell association studies revealed that the Ab-TA/PAATiO*x* NPs associated at significantly higher levels than the unmodified PAATiO*x* NPs with $CD44^+$ cells (Figures 3b, S3 and Table S4). In contrast, the association of either nanoparticle type (i.e., Ab-TA/PAATiO*x* and PAATiO*x*) with $CD44^-$ cells was negligible. Confocal microscopy further confirmed these findings, showing high CD44 surface expression (green fluorescence) on MDA-MB-231 and MIAPaCa-2 cells but not on BT-474 cells (Figures 3c and S4). Specifically, for $CD44^+$ cell lines, a stronger peak fluorescence was observed in samples with modified Ab-TA/PAATiO*x* NPs than in those with unmodified PAATiOx NPs (Figures 3b, S3 and Table S4; $p < 0.05$). The mean fluorescence intensities (MFIs) of the unmodified PAATiOx NPs were 432, 361, and 316 in MIAPaCa-2, MDA-MB-231, and BT-474 cells, respectively. In contrast, the MFIs of Ab-TA/PAATiO*x* NPs were 987, 722, and 337 in MIAPaCa-2, MDA-MB-231, and BT-474 cells, respectively, representing an approximate 2× increase for the $CD44^+$ cells. According to a previous study, the interaction between antibodies and tannic acid involves hydrogen bonding, hydrophobic interactions, and ionic interactions.[16] In Figure S4, the red and green signals represent NPs and antibody labeling, respectively. The observed yellow fluorescence within cells indicates colocalization, suggesting that the NPs were internalized while remaining conjugated with the antibodies. Although Figure S4 shows the results after 24 h of

https://doi.org/10.1021/acsabm.5c01645
ACS Appl. Bio Mater. XXXX, XXX, XXX−XXX

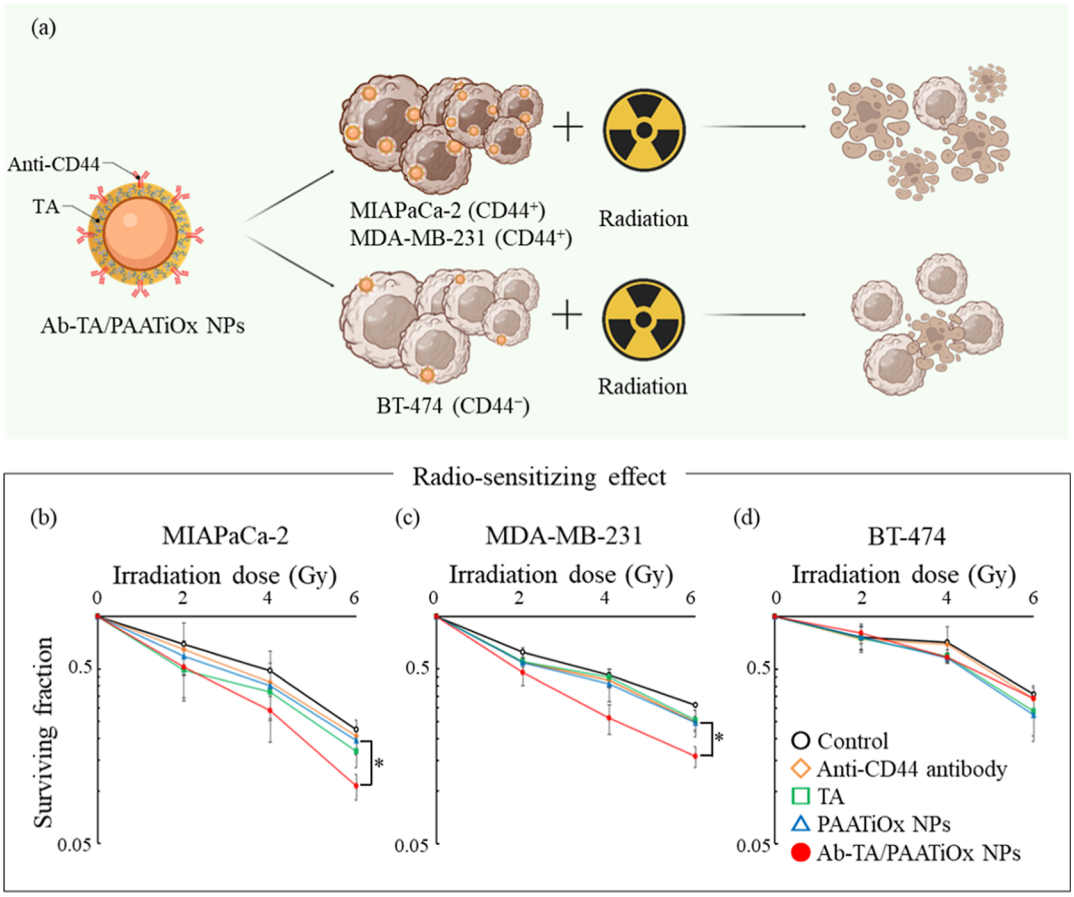

Figure 5. (a) Schematic illustration of radiation-induced cell death. (b–d) Cell death as measured by a colony-forming assay after exposure of cancer cell lines (MIAPaCa-2 (b), MDA-MB-231 (c), and BT-474 (d)) to a graded dose of X-ray radiation combined with various nanoparticle samples. Data are shown as the mean ± standard deviation and $n = 3$. Differences between groups were analyzed using the Kruskal–Wallis test with Mann–Whitney U test ($^*p < 0.05$).

coincubation, Figure S5 presents the time-dependent dissociation profile of antibodies from Ab-TA/PAATiOx NPs in RPMI-1640 medium. The results showed that ∼2% of antibodies were released from the NPs after 1 h of incubation in Milli-Q water, while ∼3% were released after 24 h of incubation in RPMI-1640 medium. In NPs incubated with RPMI-1640 medium, approximately 2–4% of antibody release was observed between 1 and 24 h. These results demonstrate that the antibodies on the surface of Ab-TA/PAATiOx NPs remain stably associated with the NPs for at least 24 h, even under physiological environment.

Fluorescence microscopy showed that the unmodified PAATiOx NPs had limited uptake in all cell lines. However, after modification, the Ab-TA/PAATiOx NPs showed high accumulation in the $CD44^+$ cell line and negligible uptake of $CD44^-$ cell line (Figure 3c).[25] ImageJ analysis revealed that the Ab-TA/PAATiOx NPs accumulated at approximately 20-fold higher concentration in $CD44^+$ cells versus $CD44^-$ cells (Figure 3d; $p < 0.05$). This difference in cellular accumulation underscores the effectiveness of our targeting strategy and supports our hypothesis that antibody-functionalized NPs would exhibit enhanced cell-specific uptake.

Having established the cell-specific targeting ability of the Ab-TA/PAATiOx NPs, we investigated their intracellular trafficking. Specifically, the endosomal/lysosomal compartments were labeled with Lysotracker and FITC-labeled anti-CD44 antibodies were used to prepare Ab-TA/PAATiOx to enable visualization by confocal microscopy. A strong overlap was observed between the NPs and endosome/lysosomes in $CD44^+$ cells (Figure 4), suggesting colocalization in these organelles. This is typical for many NPs internalized by cancer cells through endocytosis and suggests that the internalization mechanism through endocytosis is not influenced by surface modification of the PAATiOx NPs.[26]

PAATiOx NPs exhibit antitumor and radiosensitizing effects in combination with X-rays, as we have previously reported.[10,27−29] To examine the properties of the modified NPs (Ab-TA/PAATiOx), a colony-formation assay was performed on different cell lines that were treated with Ab-TA/PAATiOx and then exposed to various levels of X-ray radiation (Figure 5a). The Ab-TA/PAATiOx NPs group exhibited significant radiation enhancement in $CD44^+$ cells compared to other treatment groups (Figure 5b,c). In MIAPaCa-2 cells, the fraction of surviving cells after irradiation at 6 Gy was 0.22, 0.21, 0.17, 0.19, and 0.11 for the phosphate-buffered saline (PBS) (Control), anti-CD44 antibody, TA, PAATiOx NPs, and Ab-TA/PAATiOx NPs treatment groups, respectively (Figure 5b; $^*p < 0.05$). In MDA-MB-231 cells, the fraction of surviving cells after irradiation at 6 Gy irradiation was 0.31, 0.25, 0.25, 0.25, and 0.16 for the PBS, anti-CD44 antibody, TA, PAATiOx NPs, and Ab-TA/PAATiOx NPs treatment groups, respectively (Figure 5c; $^*p < 0.05$). In all $CD44^+$ cell lines tested, the cell survival fraction decreased with increasing radiation dose, in the controls and particles

https://doi.org/10.1021/acsabm.5c01645
ACS Appl. Bio Mater. XXXX, XXX, XXX−XXX

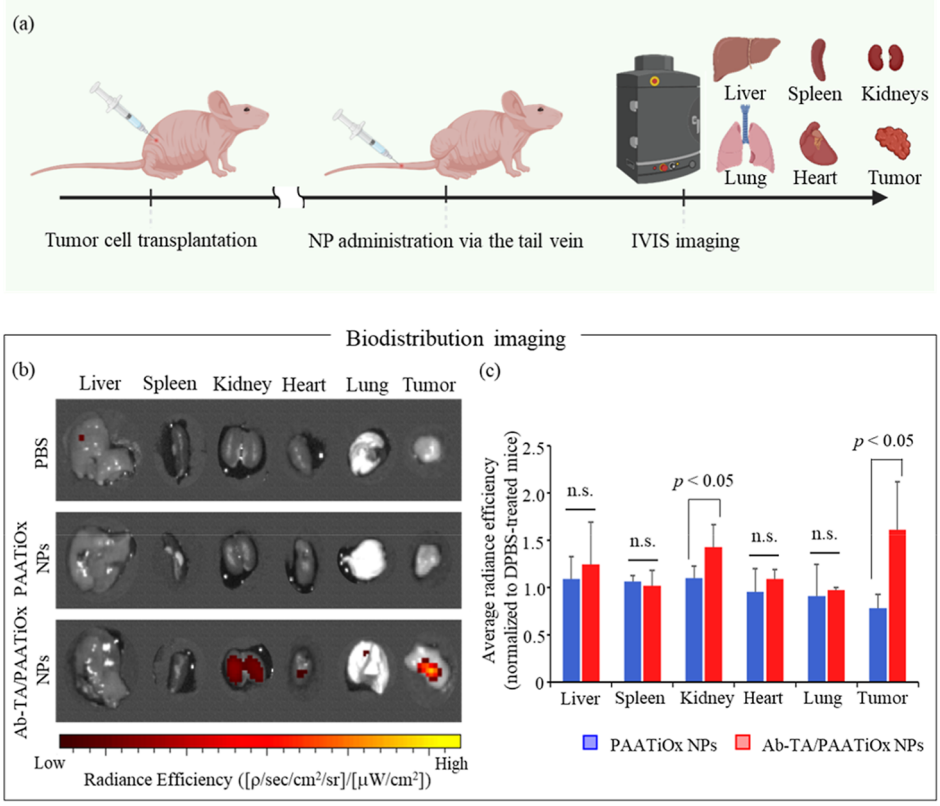

Figure 6. (a) Tumor targeting analysis in vivo. (b) Biodistribution of NPs and (c) normalized radiance efficiency in CD44-positive tumor xenografts and select organs. Data are acquired 4 h post intravenous administration of Ab-TA/PAATiO*x* or PAATiO*x* NPs in BALB/c nude mice (NPs dosage: 25 mg/kg-bodyweight). Data are shown as the mean ± standard deviation and $n = 3$. Differences between groups were analyzed using the Kruskal−Wallis test with Mann−Whitney *U* test. Results were considered significant at $p < 0.05$.

regardless of antibody coating. However, as expected, these enhanced effects were not observed in CD44-deficient cells, as accumulation was minimal. In $CD44^-$ cell line, the fraction of surviving cells after irradiation at 6 Gy was 0.36, 0.34, 0.29, 0.27, and 0.34 for the PBS, anti-CD44 antibody, TA, PAATiO*x* NPs, and Ab-TA/PAATiO*x* NPs treatment groups, respectively (Figure 5d; $p > 0.05$). Specifically, compared to the unmodified NPs, the Ab-TA/PAATiO*x* NPs exhibited significant radiosensitizing effects on $CD44^+$ cells (MIAPaCa-2 and MDA-MB-231) and resulted in greater clonogenic inhibition. Notably, $CD44^-$cells did not exhibit these effects. Importantly, the extracellular NPs were washed away after 30 min of incubation and prior to X-ray irradiation, which explains why such limited enhancement was seen for PAATiO*x* NPs in comparison to our previous studies where washing only was conducted after irradiation.[10] In the present study, the unmodified PAATiO*x* NPs barely outperformed the control groups, which highlights the importance of specific cell targeting, binding, and internalization. From the perspective of radiotherapy, the concept of combining polyphenol−metal coordination with radiation-induced oxidative mechanisms represents a next-generation approach for enhancing therapeutic efficacy. As recently reported, the incorporation of metal−phenolic chemistry into nanosystems can modulate both tumor immunogenicity and ROS-mediated damage, leading to synergistic immuno-radiotherapeutic effects.[30,31] Our findings, showing a 2-fold enhancement of tumor accumulation and radiosensitizing efficacy, are consistent with these mechanistic insights, suggesting that antibody modification primarily enhances active targeting while maintaining the redox capacity of TiO*x* NPs. Finally, these results suggested that the radiosensitizing effects of PAATiO*x* NPs were not compromised by Ab-TA surface modification.

In vivo experiments with $CD44^+$ tumor xenografts in BALB/c nude mice showed that the fluorescence signal from Ab-TA/PAATiO*x* NPs was more concentrated in the tumor than the fluorescence signal from the PAATiO*x* NPs (Figures 6a and S6). Quantitative analysis of biodistribution showed that in mice treated with Ab-TA/PAATiO*x* NPs, the average radiance efficiency was 1.25, 1.02, 1.43, 1.01, 0.97, and 1.61 in the liver, spleen, kidneys, heart, lung, and tumor, respectively, compared with 1.09, 1.07, 1.10, 0.95, 0.91, and 0.78 in the corresponding organs of mice treated with PAATiO*x* NPs. Notably, tumors treated with Ab-TA/PAATiO*x* NPs showed a 2-fold stronger fluorescence intensity than those treated with PAATiO*x* NPs, 4 h post intravenous administration (Figure 6b,c, $*p < 0.05$). NPs modified with anti-CD44 accumulate in tumor cells after administration likely owing to their antigen binding properties and internalization by $CD44^+$ tumor cells. In addition, fluorescent nanoprobes and nanotheranostic systems have been extensively explored for in vivo imaging and tumor tracking.[32−35] In agreement with these reports, the present study demonstrates that Ab−TA/PAATiO*x* NPs enable clear visualization of whole-body biodistribution and tumor accumulation, further supporting their potential as diagnostic−therapeutic (theranostic) agents. Therefore, Ab-TA functionalization using anti-CD44 may be a promising therapeutic strategy to improve antitumor efficacy.

To evaluate the potential systemic toxicity of the NPs—particularly in the liver and kidneys, where NPs tend to

https://doi.org/10.1021/acsabm.5c01645
ACS Appl. Bio Mater. XXXX, XXX, XXX−XXX

accumulate—serum biochemical analyses were conducted using blood samples collected from treated mice. Key biomarkers of liver function, including aspartate aminotransferase (AST), alanine aminotransferase (ALT), alkaline phosphatase (ALP), lactate dehydrogenase (LDH), leucine aminopeptidase (LAP), and γ-glutamyltransferase (γ-GT), as well as kidney function markers, such as blood urea nitrogen (UN) and creatinine (CRE), were measured. As summarized in Table S5, no statistically significant differences in these biomarker levels were observed between the control group and the groups treated with PAATiO*x* NPs or Ab-TA/PAATiO*x* NPs. These results indicate that both nanoparticle formulations exhibit minimal hepatotoxicity and nephrotoxicity under the tested conditions.

In summary, anti-CD44 modification resulted in approximately 2-fold increases in Ab-TA/PAATiO*x* NPs accumulation in $CD44^+$ cancer cells in vitro compared to PAATiO*x* NPs ($p < 0.05$). A 2-fold higher radiosensitizing effect in $CD44^+$ cells compared to $CD44^-$ cells ($p < 0.05$) was also observed in vitro. Notably, in vivo, the Ab-TA/PAATiO*x* NPs accumulated 2-fold more in $CD44^+$ tumor tissues compared to the PAATiO*x* NPs ($p < 0.05$). The approximately 2-fold increase in both in vitro uptake by $CD44^+$ cells and in vivo tumor accumulation of Ab-TA/PAATiO*x* NPs suggests that antibody-mediated targeting is the primary factor driving this enhancement. In vitro, the increased uptake in $CD44^+$ cells can be attributed to the specific interaction between the anti-CD44 antibody and the CD44 antigen on the cell surface.[36,37] In vivo, while nanoparticle tumor localization may be partially influenced by the passive enhanced permeability and retention (EPR) effect,[38,39] the observation that the fold increase is similar between in vitro and in vivo experiments indicates that active targeting via antibody−antigen recognition predominates. Moreover, characteristics of the tumor microenvironment, such as vascular permeability, interstitial pressure, and local tissue retention, may further modulate nanoparticle accumulation.[40] These factors likely provide a supplementary contribution to passive accumulation, further enhancing the tumor localization of antibody-modified NPs. Taken together, these findings indicate that the observed tumor accumulation of Ab-TA/PAATiO*x* NPs is primarily driven by active targeting, with passive mechanisms playing a secondary role.

We employed a CD44-targeted surface coating to facilitate the delivery of PAATiO*x* NPs into cancer stem cells. The improved pharmacokinetics and enhanced radiosensitizing efficacy of Ab-TA/PAATiO*x* NPs showcased the potential of the PPNs strategy for nanoparticle-based drug delivery systems. Beyond anti-CD44 antibodies, other targeting antibodies, such as those against CD133 or CD24, could also be applied using our versatile one-step assembly platform to broaden the spectrum of cancer targets.

CONCLUSIONS

In conclusion, this study demonstrated an antibody-functionalized nanoparticle platform for the targeted radiosensitization of $CD44^+$ cancer cells. The enhanced tumor accumulation and radiosensitizing effects demonstrated by the Ab-TA/PAATiO*x* NPs highlight the potential of this approach to improve radiotherapy outcomes through specific targeting of cancer cells, particularly cancer stem cells known to contribute to treatment resistance and disease recurrence. This strategy offers a promising approach to enhance the specificity and efficacy of radiation therapy while potentially reducing side effects associated with conventional radiotherapy approaches. Furthermore, recent molecular engineering studies have demonstrated that plant-derived polyphenols can be used to design materials with controllable photophysical and biochemical properties.[41] These advances highlight the multifunctionality of phenolic materials and suggest their potential applications in enhancing conventional DDS-based therapies, regulating intracellular redox processes, or enabling light-activated therapeutic modalities.

MATERIALS AND METHODS

Materials. Titanium dioxide (TiO_2) NPs (NPs) (STS-01) were purchased from Ishihara Sangyo Ltd. (Japan). Fluorescein isothiocyanate (FITC)-labeled anti-CD44 antibody ([IM7] [ab218749]) and nonlabeled anti-CD44 antibody ([ab157107]) were purchased from Abcam (USA). Dulbecco's phosphate-buffered saline (DPBS), minimum essential medium Eagle (MEM), Rhodamine 800 (Rh800), and antihuman immunoglobulin G (IgG)-FITC antibody were purchased from Sigma-Aldrich Co. LLC. (UK), Penicillin−streptomycin (PS), Hanks' balanced salt solution (HBSS), Alexa Fluor 647 hydrazide (AF647), carboxy-H_2DCFDA (c-H_2DCFDA), Hoechst 33342, and LysoTracker Red DND-99 were purchased from Thermo Fisher Scientific (USA). Tannic acid (TA) was purchased from Nacalai Tesque, INC. (Japan). RPMI-1640 medium and poly(acrylic acid) (PAA, molecular weight = 5 kDa) were acquired from Wako (Japan). Aminophenyl fluorescein (APF) was purchased from Goryo Chemical, INC. (Japan). Ultrapure water with a resistivity exceeding 18.2 MΩ cm was obtained from a three-stage Millipore Milli-Q plus 185 purification system (Millipore Corporation, USA). Fetal bovine serum (FBS) and trypsin-ethylenediaminetetraacetic acid were obtained from Gibco (USA).

Synthesis of TiO*x*, PAATiO*x*, and Ab-TA/PAATiO*x* NPs. Titanium peroxide (TiO*x*) NPs were synthesized from anatase-type TiO_2 NPs via H_2O_2 processing.[11,42] To prevent aggregation, the particle surfaces were modified using PAA, yielding PAATiO*x* NPs.[10] Ab-TA/PAATiO*x* NPs were obtained by modifying the PAATiO*x* NPs with an antibody−polyphenol system[16] (Figure 1a). PAATiO*x* NPs were first dispersed in Milli-Q Water (300 μL, 15 mg mL^{-1}). Then, TA solution (20 μL, 4 mg mL^{-1}; Milli-Q water) was added and incubated with the particles for 10 min under gentle shaking. An FITC-labeled anti-CD44 antibody, nonlabeled anti-CD44 antibody, or FITC-labeled antihuman IgG (20 μL, 0.5 mg mL^{-1}) was then added. The mixture was incubated in an Eppendorf thermomixer at 37 °C and 1400 rpm for 4 h. To remove excess antibodies and TA, the mixture was centrifuged at 10000*g* for 10 min and the nanoparticle pellets washed with Milli-Q water. The resultant Ab-TA/PAATiO*x* NPs were finally dispersed in Milli-Q water for future use. For fluorescence labeling, PAATiO*x* NPs solutions (300 μL, 15 mg mL^{-1}; PBS) were allowed to react with AF647 solution (30 μL, 5 mg mL^{-1}; Milli-Q water) for 1 h at 25 °C to generate AF647 labeled-PAATiO*x* NPs.

Characterization. Transmission electron microscopy were conducted on an FEI Tecnai TF20 instrument (USA) at an operating voltage of 200 kV. Transmission electron microscopy samples were prepared by dropping an aliquot (5 μL) of diluted nanoparticle suspensions onto Formvar carbon-coated copper grids. Hydrodynamic diameter and zeta-potential measurements of NPs were carried out in water using a Malvern Zetasizer Nano ZS instrument (Malvern Instruments, Worcestershire, UK).

Evaluation of Reactive Oxygen Species Production. The generation of ROS from the NPs in response to X-ray irradiation was quantitatively assessed in a cell-free system. Hydroxyl radical production was measured using APF, a fluorescent probe that selectively responds to hydroxyl radicals. APF (5 μM) was added to the PAATiO*x* NPs, TA/PAATiO*x* NPs or Ab-TA/TiO*x* NPs at various concentrations in 96-well plates. The plates were then irradiated with varying doses of X-rays (0, 5, and 10 Gy) using an MBR-1505R2 instrument (Hitachi, Tokyo, Japan) at a voltage of 150

https://doi.org/10.1021/acsabm.5c01645
ACS Appl. Bio Mater. XXXX, XXX, XXX−XXX

kV and current of 5 mA with a 1 mm-thick aluminum filter (0.5 Gy min^{-1} at the target). Fluorescence intensity was measured using a multiwell plate reader (Fluoroskan Ascent FL, Thermo Fisher Scientific Inc., MA, USA) at excitation/emission wavelengths of 490/515 nm. Hydrogen peroxide (H_2O_2) generation was evaluated using c-H_2DCFDA. C−H_2DCF (50 μM) was added to NP suspensions, followed by X-ray irradiation. The resulting fluorescence signal was detected at excitation/emission wavelengths of 485/612 nm.

Stability Evaluation of Ab-TA/PAATiO*x* NPs by Flow Cytometry. To evaluate the stability of Ab-TA/PAATiOx NPs under physiological conditions, Ab-TA/PAATiOx NPs synthesized using FITC-labeled antibodies and AF647-labeled PAATiOx NPs were dispersed in RPMI-1640 (supplemented with 10% FBS, phenol red−free) and incubated for 1, 4, and 24 h. The quantitative fluorescence distribution of the NPs was then analyzed using a CytoFLEX flow cytometer (Beckman Coulter, USA).

Loading Efficiency of Antibodies. To evaluate the loading efficiency of the incorporated antibody, Ab-TA/PAATiO*x* NPs synthesized using FITC-labeled antibodies were incubated in 500 μL of Milli-Q water for 1 h. The suspensions were then centrifuged (10,000*g*, 10 min), and 400 μL of the supernatant was collected. The amount of unbound antibody in the supernatant was quantified using a plate reader at excitation/emission wavelengths of 491/516 nm. The antibody loading efficiency (%) was calculated using the following equation

$$\text{loading efficiency (\%)} = (1 - F_{\text{supernatant}}/F_{\text{initial}}) \times 100$$

where $F_{\text{supernatant}}$ and F_{initial} represent the fluorescence intensity of FITC-labeled antibodies before and after nanoparticle synthesis, respectively.

Cell Culture. Human mammary gland cancer cell lines MDA-MB-231 and BT-474 were purchased from the American Type Culture Collection (Manassas, VA, USA) and the human pancreatic cancer cell line MIAPaCa-2 was purchased from the Japanese Collection of Research Bioresources Cell Bank (Osaka, Japan). MDA-MB-231 cells and BT-474 cells were cultured in RPMI-1640 medium comprising 10% FBS and 1% PS. MIAPaCa-2 cells were cultured in MEM comprising 10% FBS and 1% PS. All cell lines were incubated at 37 °C in a humidified incubator with 5% CO_2 and 95% relative humidity.

Preparation of Cells for Treatment. MIAPaCa-2, MDA-MB-231, and BT-474 cells were seeded at 5×10^5 cells per 10 cm dish and cultured in RPMI-1640 medium or MEM for 24 h at 37 °C. Cells were collected in a 1.5 mL Eppendorf tube using a cell scraper, washed in PBS, and centrifuged at 2000 rpm for 5 min. Cell pellets were retained for subsequent analyses and after removing the supernatant.

Measurement of CD44 Expression Levels by Fluorescence-Activated Cell Sorting (FACS). Cells were incubated with FITC-labeled anti-CD44 antibody for 30 min and then subjected to flow cytometry analysis to measure CD44 expression. Controls were prepared without anti-CD44 antibodies. After incubation, cells were washed with PBS and centrifuged (2000 rpm, 5 min), then suspended in PBS. A BD FACSVerse flow cytometer (BD Biosciences, USA) was used to measure forward scatter (FSC), side scattering (SSC), and fluorescence signals. Data were analyzed using cell Quest Pro Software (version 5.1, BD Biosciences, USA).

Cellular Association Analysis by Flow Cytometry. The cultured cells were mixed with solutions of Ab-TA/PAATiO*x* NPs or PAATiO*x* NPs and incubated for 30 min at 37 °C to evaluate NP uptake. To remove excess proteins and free AF647, cells were washed with PBS, centrifuged three times for 5 min each at 2000 rpm, then suspended in PBS. Flow cytometry (BD FACSVerse, BD Biosciences, USA) and Cell Quest Pro software (version 5.1, BD Biosciences, USA) were used respectively to measure and analyze fluorescence.

Cellular Uptake Analysis by Confocal Microscopy. Cells were incubated with Ab-TA/PAATiO*x* NPs, PAATiO*x* NPs, or anti-CD44 antibody for 30 min at 37 °C. After incubation, cells were washed with PBS and centrifuged three times (2000 rpm, 5 min), then seeded into glass-bottom dishes and cultured in their respective media for 24 h at 37 °C. Cells were gently washed with DPBS three times and fixed with 4% paraformaldehyde in DPBS for 20 min at 25 °C in the dark. After fixation, cells were washed again with HBSS three times and stained with Hoechst 33342 (2 μg mL^{-1}) for 5 min at 25 °C. Cellular uptake of NPs was observed using a confocal microscope (LSM700, Carl Zeiss AG, Germany) with an oil immersion objective lens at 40× magnification. Images were analyzed using a ZEN 2012 software (Carl Zeiss AG) and processed using ImageJ (version 1.52; National Institutes of Health). Analyses were performed on a median of 30 cells per condition.

Evaluation of Endocytosis of Ab-TA/PAATiO*x* NPs. To confirm that Ab-TA coating did not interfere with endocytosis, cells were incubated with Ab-TA/PAATiO*x* NPs or anti-CD44 antibody for 30 min at 37 °C. After incubation, the cells were washed with PBS and centrifuged (2000 rpm, 5 min), seeded into glass-bottom dishes, and cultured for 24 h at 37 °C. Cells were then washed with DPBS three times and stained with LysoTracker Red DND-99 according to the manufacturer's instructions before being observed under an LSM700 microscope.

Colony-Formation Assay. Cells were incubated with PBS (1.5 mL), PAATiO*x* NPs (1.5 mL, 1.3 mg mL^{-1}; medium), TA (1.5 mL; 17 μg mL^{-1}, medium), anti-CD44 antibodies (1.5 mL; 2.2 μg mL^{-1}, medium), or Ab-TA/PAATiO*x* NPs (1.5 mL, 1.3 mg mL^{-1}; medium) for 30 min at 37 °C. After incubation, cells were washed with PBS, centrifuged (2000 rpm, 5 min) three times and seeded into six-well plates. Cells were irradiated with X-ray doses of 0, 2, 4, and 6 Gy using an MBR-1505R2 instrument at a voltage of 150 kV and current of 5 mA with a 1 mm-thick aluminum filter (0.5 Gy min^{-1} at the target). After 12 days, colonies were fixed with a solution of 10% methanol and 20% acetic acid, stained with methylene blue and counted under a light microscope. The hypothesized mechanisms of cell death is illustrated in Figure 1b.

In Vivo Biodistribution of NPs. All animal experiments were approved and performed in accordance with the Kobe University Animal Experimentation Regulations (approval number: P230905). Male C57BL/6J mice (7−10 weeks old) were obtained from CLEA Japan, Inc. (Japan) and housed under standard conditions (12 h light/dark cycle with ad libitum access to food and water). For tumor-bearing mouse studies, MDA-MB-231 cells (5×10^6) were injected into the flank region of BALB/c nude mice. When tumor volumes reached ∼100 mm^3 (calculated according to the formula volume = $1/2 \times L \times W^2$, wherein L and W are the tumor dimensions at the longest and widest points, respectively), mice were randomly divided into groups of three. Each group received intravenous injections (100 μL via the lateral tail vein) of either AF647-labeled PAATiO*x* NPs, Ab-TA/PAATiO*x* NPs (25 mg per kg body weight), or DPBS (control). A limitation of this study is the small sample size in the animal experiments (n = 3 per group), which may not be sufficient to achieve statistical significance. Mice were euthanized 4 h post administration, and the liver, spleen, kidneys, heart, lung and tumor were harvested for imaging. Far-red fluorescence signal from each organ was captured using a Xenogen IVIS 200 system. The normalized average radiance efficiency of each organ was calculated using the following equation

$$I_{\text{normalized}} = I_{\text{NP}}/I_{\text{DPBS}}$$

where $I_{\text{normalized}}$ is the normalized average radiance efficiency of the select organ, I_{NP} is the average radiance efficiency of the organ in the Rh800-labeled NP-treated mice, and I_{DPBS} is the average radiance efficiency of the organ in the DPBS-treated mice.

Statistical Analysis. Data are presented as mean ± standard deviation. Statistical analyses were performed using the EZR software (version 1.55; Saitama Medical Center, Jichi Medical University, Saitama, Japan) on R commander (version 2.7−1; the sociology department at McMaster University, Hamilton, Ontario, Canada).[43] Differences between groups were analyzed using the Kruskal−Wallis test with Mann−Whitney U test. Results were considered significant at $p < 0.05$.

Minimum Information Reporting in Bio−Nano Experimental Literature (MIRIBEL). The studies conducted herein, including

https://doi.org/10.1021/acsabm.5c01645
ACS Appl. Bio Mater. XXXX, XXX, XXX−XXX

material characterization, biological characterization, and experimental details, conform to the MIRIBEL reporting standard for bio−nano research, and we include a companion checklist of these components.

■ ASSOCIATED CONTENT

Data Availability Statement

Research data are stored in an institutional repository and will be shared upon request to the corresponding author.

Supporting Information

The Supporting Information is available free of charge at https://pubs.acs.org/doi/10.1021/acsabm.5c01645.

Figures and tables related to experimental design, nanoparticle surface modification, antibody coating, cellular uptake, and in vivo distribution are available. Figures S1−S6 include evaluation of nanoparticle surface modifications (S1), CD44 antigen expression levels in various cell lines measured by FITC-anti-CD44 flow cytometry (S2), mean fluorescence intensity (MFI) of cells incubated with PAATiOx or Ab-TA/PAATiOx NPs (S3), representative fluorescence microscopy images of nanoparticle uptake by CD44-positive (MIAPaCa-2, MDA-MB-231) and CD44-negative (BT-474) cells (S4), fluorescence distributions of NPs and free antibodies measured by flow cytometry (S5), and in vivo accumulation of NPs at tumor sites assessed by IVIS imaging in mice (S6). Tables S1−S5 provide information on loading of anti-CD44 antibodies on PAATiOx NPs (S1), fluorescence labeling and evaluation of Ab-TA coating on PAATiO*x* NPs (S2), CD44 expression levels in cancer cell lines (S3), cellular binding of PAATiO*x* or Ab-TA/PAATiO*x* NPs (S4), and blood test analyses following nanoparticle administration (S5) (PDF)

■ AUTHOR INFORMATION

Corresponding Author

Ryohei Sasaki − *Division of Radiation Oncology, Kobe University Hospital, Kobe 650-0017, Japan*; Phone: +81-78-382-5687; Email: rsasaki@med.kobe-u.ac.jp; Fax: +81-78-382-6734

Authors

Hiroaki Akasaka − *Division of Radiation Oncology, Graduate School of Medicine, Kobe University, Kobe 650-0017, Japan*; orcid.org/0000-0003-1017-5229

Makiko Nakahana − *Division of Radiation Oncology, Graduate School of Medicine, Kobe University, Kobe 650-0017, Japan*

Masao Nakayama − *Division of Radiation Therapy, Kita-Harima Medical Center, Ono, Hyogo 675-1392, Japan*

Kenta Morita − *Department of Chemical Science and Engineering, Graduate School of Engineering, Kobe University, Kobe 657-8501, Japan*; orcid.org/0000-0002-2156-4812

Mohammed Salah − *Division of Radiation Oncology, Graduate School of Medicine, Kobe University, Kobe 650-0017, Japan; Department of Biochemistry, Faculty of Veterinary Medicine, Qena University, Qena 83522, Egypt*

Naritoshi Mukumoto − *Division of Radiation Oncology, Kobe University Hospital, Kobe 650-0017, Japan*

Yasuyuki Shimizu − *Division of Radiation Oncology, Kobe University Hospital, Kobe 650-0017, Japan*

Ruixain Zhangzhu − *Division of Radiation Oncology, Graduate School of Medicine, Kobe University, Kobe 650-0017, Japan*

Chiaki Ogino − *Department of Chemical Science and Engineering, Graduate School of Engineering, Kobe University, Kobe 657-8501, Japan*; orcid.org/0000-0002-8906-7724

Christina Cortez-Jugo − *Department of Chemical Engineering, The University of Melbourne, Parkville, Victoria 3010, Australia*; orcid.org/0000-0001-5341-175X

Joseph J. Richardson − *School of Engineering, RMIT University, Victoria 3001, Australia*

Frank Caruso − *Department of Chemical Engineering, The University of Melbourne, Parkville, Victoria 3010, Australia*; orcid.org/0000-0002-0197-497X

Complete contact information is available at: https://pubs.acs.org/10.1021/acsabm.5c01645

Funding

This work was supported by a Grants-in-Aid for Exploratory Research (no. 25K22612, RS), Scientific Research (C) (no. 22K07771, HA, 24K10910, MN, 23K07061, NM, 25K10962, YS), Fund for the Promotion of Joint International Research (no. 23KK0282, HA), or and Research Fellowship for Young Scientists (no. 24KJ0166, HA) from the Ministry of Education, Culture, Sports, Science, and Technology of Japan and was partly funded under an Australian Research Council Discovery Project scheme (DP210103114, FC).

Notes

The authors declare no competing financial interest.

■ ABBREVIATIONSP

γ-GT, γ-glutamyltransferase; AF647, Alexa Fluor 647; ALP, Alkaline phosphatase; ALT, alanine aminotransferase; APF, aminophenyl fluorescein; AST, Aspartate aminotransferase; Ab-TA, antibody−tannic acid; c-H2DCFDA, carboxy-2′,7′-dichlorodihydrofluorescein diacetate; CRE, creatinine; DLS, dynamic light scattering; DPBS, Dulbecco's phosphate-buffered saline; EPR, enhanced permeability and retention; FBS, fetal bovine serum; FITC, fluorescein isothiocyanate; HBSS, Hanks' balanced salt solution; IgG, immunoglobulin G; LAP, Leucine aminopeptidase; LDH, Lactate dehydrogenase; MEM, minimum essential medium Eagle; MPN, metal−phenolic networks; MQ, Milli-Q; PAATiO*x* NPs, polyacrylic acid-modified titanium peroxide NPs; PBS, phosphate-buffered saline; PDI, polydispersity index; PPNs, polypeptide−polyphenol networks; PS, penicillin-streptomycin; Rh800, Rhodamine 800; TA, tannic acid; TiO2, titanium dioxide; UN, urea nitrogen.

■ REFERENCES

(1) Akasaka, H.; Mukumoto, N.; Nakayama, M.; et al. Investigation of the potential of using TiO2 nanoparticles as a contrast agent in computed tomography and magnetic resonance imaging. *Appl. Nanosci* **2020**, *10*, 3143−3148.

(2) Chen, H. H. W.; Kuo, M. T. Improving radiotherapy in cancer treatment: Promises and challenges. *Oncotarget* **2017**, *8* (37), 62742−62758.

(3) Baumann, M.; Krause, M.; Overgaard, J.; Debus, J.; Bentzen, S. M.; Daartz, J.; Richter, C.; Zips, D.; Bortfeld, T. Radiation oncology in the era of precision medicine. *Nat. Rev. Cancer* **2016**, *16* (4), 234.

(4) Le, Q. T.; Shirato, H.; Giaccia, A. J.; Koong, A. C. Emerging Treatment Paradigms in Radiation Oncology. *Clin. Cancer Res.* **2015**, *21* (15), 3393.
(5) Akasaka, H.; Sasaki, R.; Miyawaki, D.; et al. Preclinical evaluation of bioabsorbable polyglycolic acid spacer for particle therapy. *Int. J. Radiat Oncol Biol. Phys.* **2014**, *90* (5), 1177−1785.
(6) Yang, L.; Shi, P.; Zhao, G.; et al. Targeting cancer stem cell pathways for cancer therapy. *Signal Transduct Target Ther* **2020**, *5* (1), 8.
(7) Ma, N.; Jiang, Y. W.; Zhang, X.; et al. Enhanced radiosensitization of gold nanospikes via hyperthermia in combined cancer radiation and photothermal therapy. *ACS Appl. Mater. Interfaces* **2016**, *8* (42), 28480−28494.
(8) Ma, N.; Wu, F. G.; Zhang, X.; et al. Shape-dependent radiosensitization effect of gold nanostructures in cancer radiotherapy: of gold nanoparticles, nanospikes, and nanorods. *ACS Appl. Mater. Interfaces* **2017**, *9* (15), 13037−13048.
(9) Jiang, Y. W.; Gao, G.; Jia, H. R.; et al. Copper oxide nanoparticles induce enhanced radiosensitizing effect via destructive autophagy. *ACS Biomater. Sci. Eng.* **2019**, *5* (3), 1569−1579.
(10) Nakayama, M.; Sasaki, R.; Ogino, C.; et al. Titanium peroxide nanoparticles enhanced cytotoxic effects of x-ray irradiation against pancreatic cancer model through reactive oxygen species generation in vitro and in vivo. *Radiat Oncol* **2016**, *11* (1), 91.
(11) Morita, K.; Miyazaki, S.; Numako, C.; et al. Characterization of titanium dioxide nanoparticles modified with polyacrylic acid and H_2O_2 for use as a novel radiosensitizer. *Free Radical Res.* **2016**, *50* (12), 1319−1328.
(12) Nishimura, Y.; Ezawa, R.; Morita, K.; et al. In vivo evaluation of the Z. HER2-BNC/LP carrier encapsulating an anticancer drug and a radiosensitizer. *ACS Appl. Bio Mater.* **2020**, 3 (11), 7743−7751.
(13) Morita, K.; Suzuki, T.; Nishimura, Y.; et al. In vivo tissue distribution and safety of polyacrylic acid-modified titanium peroxide nanoparticles as novel radiosensitizers. *J. Biosci. Bioeng.* **2018**, *126* (1), 119−125.
(14) Guo, J.; Ping, Y.; Ejima, H.; Alt, K.; Meissner, M.; Richardson, J. J.; Yan, Y.; Peter, K.; von Elverfeldt, D.; Hagemeyer, C. E.; et al. Engineering multifunctional capsules through the assembly of metal-phenolic networks. *Angew. Chem., Int. Ed. Engl.* **2014**, *53* (22), 5546.
(15) Wang, Y.; He, Y.; Hong, G.; Wang, X.; Guo, J. Conversion of plant polyphenols into high-value products and multi-disciplinary applications. *Sci. Sin. Chim.* **2025**, *55* (1), 37−49.
(16) Han, Y.; Lin, Z.; Zhou, J.; et al. Polyphenol-mediated assembly of proteins for engineering functional materials. *Angew. Chem., Int. Ed. Engl.* **2020**, *59* (36), 15618−15625.
(17) Thapa, R.; Wilson, G. D. The Importance of CD44 as a Stem Cell Biomarker and Therapeutic Target in Cancer. *Stem Cells Int.* **2016**, *2016*, 2087204.
(18) Xu, H.; Tian, Y.; Yuan, X.; et al. The role of CD44 in epithelial−mesenchymal transition and cancer development. *Onco Targets Ther* **2015**, *8*, 3783.
(19) Ma, F.; Li, H.; Wang, H.; et al. Enriched CD44(+)/CD24(−) population drives the aggressive phenotypes presented in triple-negative breast cancer (TNBC). *Cancer Lett.* **2014**, *353* (2), 153.
(20) Moreira, M. P.; da Conceição Braga, L.; Cassali, G. D.; et al. STAT3 as a promising chemoresistance biomarker associated with the CD44+/high/CD24-/low/ALDH+ BCSCs-like subset of the triple-negative breast cancer (TNBC) cell line. *Exp. Cell Res.* **2018**, *363* (2), 283−290.
(21) Menke-van der Houven van Oordt, C. W.; Gomez-Roca, C.; van Herpen, C.; Coveler, A. L.; Mahalingam, D.; Verheul, H. M. W.; van der Graaf, W. T. A.; Christen, R.; Rüttinger, D.; Weigand, S.; et al. First-in-human phase I clinical trial of RG 7356, an anti-CD44 humanized antibody, in patients with advanced, CD44-expressing solid tumors. *Oncotarget* **2016**, *7* (48), 80046−80058.
(22) Jauw, Y. W. S.; Huisman, M. C.; Nayak, T. K.; et al. Assessment of target-mediated uptake with immuno-PET: analysis of a phase I clinical trial with an anti-CD44 antibody. *EJNMMI Res.* **2018**, *8* (1), 6.
(23) Ejima, H.; Richardson, J. J.; Liang, K.; et al. One-step assembly of coordination complexes for versatile film and particle engineering. *Science* **2013**, *341* (6142), 154−157.
(24) Kulkarni, S. A.; Feng, S. S. Effects of particle size and surface modification on cellular uptake and biodistribution of polymeric nanoparticles for drug delivery. *Pharm. Res.* **2013**, *30* (10), 2512.
(25) Rasband, W. S. *Imagej.*, U. S. National Institutes of Health, Bethesda, Maryland, USA, https://imagej.nih.gov/ij/, 1997-2018.
(26) Rennick, J. J.; Johnston, A. P. R.; Parton, R. G. Key principles and methods for studying the endocytosis of biological and nanoparticle therapeutics. *Nat. Nanotechnol.* **2021**, *16* (3), 266−276.
(27) Hassan, M.; Nakayama, M.; Salah, M.; et al. A Comparative Assessment of Mechanisms and Effectiveness of Radiosensitization by Titanium Peroxide and Gold Nanoparticles. *Nanomaterials (Basel)* **2020**, *10* (6), 1125.
(28) Morita, K.; Nishimura, Y.; Nakamura, S.; et al. Titanium oxide nano-radiosensitizers for hydrogen peroxide delivery into cancer cells. *Colloids Surf. B Biointerfaces* **2021**, *198*, 111451.
(29) Salah, M.; Akasaka, H.; Shimizu, Y.; et al. Reactive oxygen species-inducing titanium peroxide nanoparticles as promising radiosensitizers for eliminating pancreatic cancer stem cells. *J. Exp. Clin. Cancer Res.* **2022**, *41* (1), 146.
(30) Wang, G.; Yan, J.; Tian, H.; et al. Dual-Epigenetically Relieving the MYC-Correlated Immunosuppression via an Advanced Nano-Radiosensitizer Potentiates Cancer Immuno-Radiotherapy. *Adv. Mater.* **2024**, *36* (19), No. e2312588.
(31) Li, W.; Tian, H.; Yan, Z.; Yu, X.; Li, B.; Dai, Y. Magnesium-Phenolic Nanoeditor Refining Gliomatous T Cells for Metalloimmunotherapy. *ACS Nano* **2025**, *19* (1), 1222−1237.
(32) Prasad, R.; Chauhan, D. S.; Yadav, A. S.; et al. A Biodegradable Fluorescent Nanohybrid for Photo-Driven tumor Diagnosis and Tumor Growth Inhibition. *Nanoscale* **2018**, *10*, 19082−19091.
(33) Prasad, R.; Mendes, B. B.; Gorain, M.; et al. Bioinspired and biomimetic cancer-cell-derived membrane nanovesicles for preclinical tumor-targeted nanotheranostics. *Cell Rep. Phys. Sci.* **2023**, *4* (11), 101648.
(34) Prasad, R.; Jain, N. K.; Yadav, A. S.; et al. Liposomal nanotheranostics for multimode targeted in vivo bioimaging and near-infrared light mediated cancer therapy. *Commun. Biol.* **2020**, *3* (1), 284.
(35) Prasad, R.; Prerna, K.; Temgire, M.; et al. Molecular Engineering of Ultrabright Biomimetic NanoGhost for Site-Selective Tumor Imaging and Biodistribution. *Adv. Healthc Mater.* **2025**, *14* (3), No. e2401233.
(36) Peer, D.; Karp, J. M.; Hong, S.; et al. Nanocarriers as an emerging platform for cancer therapy. *Nat. Nanotechnol.* **2007**, *2* (2), 751−760.
(37) Jain, R. K. Normalization of tumor vasculature: an emerging concept in antiangiogenic therapy. *Science* **2005**, *307* (5706), 58−62.
(38) Maeda, H.; Wu, J.; Sawa, T.; et al. Tumor vascular permeability and the EPR effect in macromolecular therapeutics: a review. *J. Controlled Release* **2000**, *65* (1−2), 271−284.
(39) Fang, J.; Nakamura, H.; Maeda, H. The EPR effect: Unique features of tumor blood vessels for drug delivery, factors involved, and limitations and augmentation of the effect. *Adv. Drug Deliv Rev.* **2011**, *63* (3), 136−151.
(40) Blanco, E.; Shen, H.; Ferrari, M. Principles of nanoparticle design for overcoming biological barriers to drug delivery. *Nat. Biotechnol.* **2015**, *33* (9), 941−951.
(41) Yang, G.; Zhang, Y.; Lei, C.; et al. Molecular Engineering of Plant Polyphenols Into Amorphous Room-Temperature Phosphorescent Materials. *Angew. Chem., Int. Ed. Engl.* **2025**, *64* (36), No. e202511218.
(42) Kanehira, K.; Banzai, T.; Ogino, C.; Shimizu, N.; Kubota, Y.; Sonezaki, S. Properties of TiO2-polyacrylic acid dispersions with potential for molecular recognition. *Colloids Surf. B Biointerfaces* **2008**, *64*, 10−15.

https://doi.org/10.1021/acsabm.5c01645
ACS Appl. Bio Mater. XXXX, XXX, XXX−XXX

(43) Kanda, Y. Investigation of the freely available easy-to-use software 'EZR' for medical statistics. *Bone Marrow Transplant* **2013**, *48* (3), 452−458.

https://doi.org/10.1021/acsabm.5c01645
ACS Appl. Bio Mater. XXXX, XXX, XXX−XXX